

Large-scale optimization of neuron arbors

Christopher Cherniak,* Mark Changizi,† and Du Won Kang‡

Committee on History and Philosophy of Science, Department of Philosophy, University of Maryland, College Park, Maryland 20742

(Received 21 July 1998)

At the global as well as local scales, some of the geometry of types of neuron arbors—both dendrites and axons—appears to be self-organizing: Their morphogenesis behaves like flowing water, that is, fluid dynamically; waterflow in branching networks in turn acts like a tree composed of cords under tension, that is, vector mechanically. Branch diameters and angles and junction sites conform significantly to this model. The result is that such neuron tree samples globally minimize their total volume—rather than, for example, surface area or branch length. In addition, the arbors perform well at generating the cheapest topology interconnecting their terminals: their large-scale layouts are among the best of all such possible connecting patterns, approaching 5% of optimum. This model also applies comparably to arterial and river networks. [S1063-651X(99)16205-6]

PACS number(s): 87.19.-j, 87.10.+e

Brains do not grow like crystals. However, some of the architectures of a variety of types of neuron arbors seem to be similarly self-structuring. This can be predicted by a simple fluid-mechanical model, where the neural trees are represented in terms of a laminar flow of fluid through a corresponding tube network. The model applies well, for example, to planar arbors of mammalian retinal ganglion and amacrine cell dendrites, and of both intrinsic and extrinsic thalamic axons. Local branch-junction geometry conforms to a fluid-dynamical model, with branch diameters set to minimize the internal wall drag of the fluid flow, which in turn sets branch angles. The complete tree structure thereby conforms to a fluid-static model, as if its hypothetical branch tubes were all “inflated,” with the resulting vector-mechanical system behaving like a network under tension. This fluid-mechanical model predicts that a given tree will be stretched or embedded in the minimum-volume configuration connecting its terminals; neuroanatomical observations, in fact, support this conclusion. Furthermore, among the many alternative possible topologies, the actual topologies of these arbors are close to the minimum-volume ones.

The neuron arbors fit this large-scale model almost as well as nonliving tree structures such as river drainage networks, and also blood vessel anatomy (Ref. [1] reviewed the wide range of non-neural arborizations occurring in nature). This “neural fluid mechanics” provides a first approximation of an explanation of how a “save wire” generative rule [2] for network wiring optimization in the brain is in fact implemented for one aspect of neuroanatomy. Some of the significance of such an account, for instance, concerns how complex biological structure can emerge “for free” directly from simple physical phenomena [1–5]. Such self-optimizing tree structures might provide an enriched milieu for “neuromorphs”—artificial neuronlike signal processing elements [6]—that could grow their own networks.

STEINER TREE

The simplest forms of the core tree-optimization concept here have been studied at least since Fermat and Torricelli

(see, e.g., Ref. [7]). The relevant classical version of the Steiner tree problem is the following: Given a set of fixed nodes, find the set of arcs or branch segments that interconnects all nodes and has the shortest total length. The resulting network will always constitute a tree. When it is permitted to have branch junctions only at node sites, it is a *minimal spanning tree*; when branchings may also occur at loci that are not nodes, it constitutes a *Steiner tree*. The total length of the Steiner tree for a set of nodes is equal to or less than the length of the minimal spanning tree for the nodes (with a maximum possible improvement of about 13% [8]). For example, Figs. 1(A) and 1(B) show, respectively, a minimal spanning tree and a Steiner tree for five nodes on a plane; the Steiner tree has three internodal junctions j , and is about 4% shorter than the minimal spanning tree.

Steiner tree is a combinatorial optimization problem: The exact solution of a problem instance in general requires (a) generating all possible alternative connecting patterns, or topologies, among the given nodes (see, e.g., Fig. 6 below); and (b) for each topology, finding its minimum-cost embedding, that is, the best positioning of its internodal junctions. Steiner tree—unlike minimal spanning tree—has been proven to be an NP-complete problem, indeed, NP hard [9,10]. The concept of NP completeness (“nondeterministic polynomial-time completeness”) need not be defined here, but it is strongly conjectured to be linked with a problem being intrinsically computationally intractable, i.e., not generally solvable without an exhaustive search of all possible solutions. Because the number of possibilities—topologies,

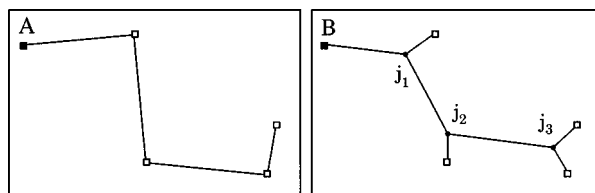


FIG. 1. Two classical models of tree optimality: (A) Minimal spanning tree, and (B) Steiner tree, for five nodes on a plane surface. The Steiner tree has internodal junctions j ; it is therefore shorter than the minimal spanning tree, but much more computationally costly to construct. The Steiner tree concept in fact applies to neuron arbors, but with the cost measure as the total tree volume, rather than the total tree length.

*Electronic address: CHERNIAK@umail.umd.edu

†Electronic address: CHANGIZI@cs.ucc.ie

‡Electronic address: DUWON@lexsolutions.com

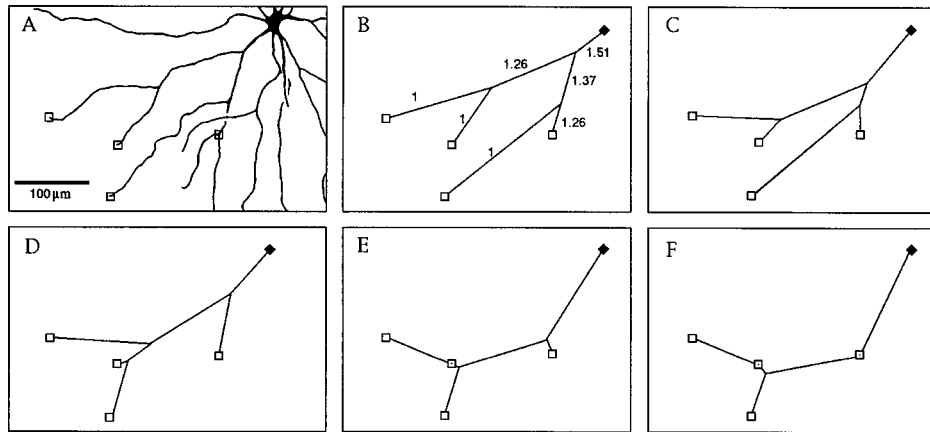


FIG. 2. Optimization analysis of a five-terminal subtree from the dendritic arbor of an α ganglion cell in rabbit retina. (A) A quadrant of the original camera lucida drawing containing the subtree (after Ref. [13], p. 29); soma is in the upper right corner. “Leaf terminals” of the analysis are boxed (note that one of them is not a branch termination); the “root terminal” is at soma. (B) Wireframe representation of the actual tree, with branch segments straightened between loci of terminals and internodal junctions. The labels give the diameters assigned to the branch segments via the power law for the laminar-flow value $p=3.00$ (with correction for branch bend in; see text). (C) Optimal (re)embedding of the topology of the actual tree, with respect to the total volume cost, via the STRETCH algorithm. This minimum-volume embedding of the actual topology is 1.06% cheaper than the volume of the actual tree in (B). (D) Optimal embedding of the optimal topology for the given terminal loci, with respect to volume cost. It can be seen to differ from the actual topology of (A)–(C). It is 2.64% cheaper in volume than the actual topology in its actual embedding in (B). (E) Optimal embedding of the optimal topology, with respect instead to the total tree surface area. The actual vs optimal error is now 27.22%, much greater. (F) Optimal embedding of the optimal topology, with respect to the total tree length. The actual vs optimal error is now 60.58%, even greater. [Some junction sites of (E) and (F) are identical with terminal sites.] Thus this dendritic arbor best fits a minimum-volume model.

in the Steiner tree case—combinatorially explodes as the size of a problem-instance grows (e.g., a ten-node tree has over two million Steiner topologies), such brute-force searches are extremely computationally costly. The largest unconstrained classical Steiner tree problems solvable at the end of the last decade had only 30 nodes [11], and today have about 100.

The basic question of the goodness of fit of the Steiner tree concept to actual neuroanatomy is the following: Do dendrites or axons form optimized Steiner trees interconnecting the cell body with a set of synaptic loci [1,12]? However, a typical dendritic or axonic arbor has thousands of synapses, a node set of unfeasible size. Instead, the analysis below treats the hierarchically next-highest-level arbor elements, the branch terminations, as the “leaf nodes” to be economically interconnected with each other, and the “root node” or origin (e.g., the cell body): for example, Fig. 2(A) shows one “bough” portion of the dendritic arbor of an α ganglion cell in rabbit retina [13] with three such branch-termination leaves. It should be noted that the fluid-mechanical account here implies that the leaf nodes are not target sites fixed in advance; rather, as the system is “inflated,” positions of the branch terminations shift into vector-mechanical equilibrium. The optimization thesis is that the resulting arbor is a Steiner tree. The account here is thus consistent with conventional conceptions of dendritic arbor structure as mainly “intrinsically” driven [14]—yielding, in effect, the most economical “synapse rack” to receive connections. In contrast, according to the conventional conception, typical axons are more “extrinsically” driven as their growth tips home on their synapse targets [15]. It is interesting, therefore, that the fluid-mechanical account here turns out to apply equally well to some types of axon (e.g., of the reticular formation); pos-

sibly these particular axons also are laid out by similarly intrinsic processes.

Because optimization of two-dimensional arbors is much better understood than that of three-dimensional ones, the analysis below concentrates on the former. The dendrite and axon trees selected as data for analysis are of highly regular types, with relatively straight branches, and no branch cross-overs [e.g., the bough of Fig. 2(A), as opposed to the tree consisting of that bough with the bough to its right]. One observation regarding network optimization is immediately salient: A classical theorem for minimal spanning trees states that no branch junction can have an angle of less than 60° , from which it follows that no node can have more than six branches. If the soma of planar neuron arbor types such as retinal ganglion cells is treated as such a node, and examples are selected with approximately symmetrical dendritic arbors and with boughs of approximately equal size, this “six-branch rule” can be tested. Peichl, Ott, and Boycott [16] includes relevant α ganglion cells of 13 mammalian species; all somata receive six or less dendrite branches, with mean $5.15 (\pm 0.80)$. The six-branch rule was similarly confirmed without exception by the α ganglion cells from rabbit retina by Peichl, Buhl, and Boycott [13].

LOCAL Y TREES

Fluid dynamics. The classical Steiner tree concept cannot be applied further to natural tree structures because, while the usual Steiner tree formalism treats all segments as equal, typically trunks of natural trees—living and nonliving—have greater diameter than their branches. The concept of a *variably weighted* Steiner tree is therefore required, where segments need not have uniform cost per unit length. We begin with the local analysis of single internodal junction “Y

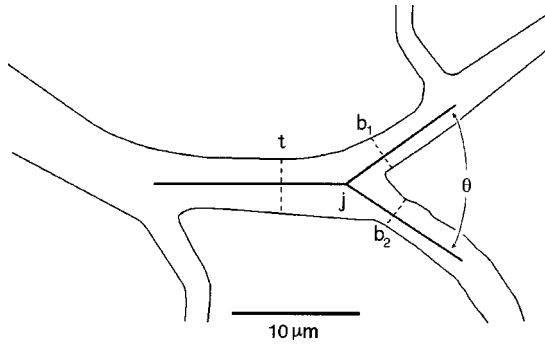


FIG. 3. Bifurcating junction in a neuron arbor: t , trunk; b_1 and b_2 , branches; j , internodal junction; θ , internal branch angle. The “Y”-tree diagram is superimposed upon a simplified outline of a junction in the data set from the dendritic arbor of a δ ganglion cell in cat retina. The neuron arbor junction trunk and branch diameters conform to the power law $t^p = b_1^p + b_2^p$, with $p \cong 3$; this is a fluid-dynamic model for the minimum internal wall drag of pumped flow under a laminar regime through a pipe junction. In turn, the internal branch angles of the neuron junctions conform to the “triangle of forces” law $\cos \theta = (w_t^2 - w_{b1}^2 - w_{b2}^2) / 2w_{b1}w_{b2}$, with weights w_n corresponding to cross-section areas of respective trunk and branches; this vector-mechanical model yields minimum volume of a Y-tree junction.

trees,” the components of complex trees. First, a model of the relation of branch costs to their trunk cost is necessary. One promisingly general candidate can be drawn from fluid dynamics: Originating with Murray’s [17] work on vascular arbors, the “cube law” states that, for diverging flow from trunk to branches at an arterial junction, tube-wall drag of the moving fluid is minimized if inside diameters of the trunk and branches fit a relationship that the cube of trunk diameter equals the sum of cubed diameters of all branches (see Fig. 3). This derivation holds for laminar flow, that is, typically, fluid moving smoothly in tubes of one millimeter diameter or less, at velocities low enough not to induce eddy disturbances [18]. In general, it has been well confirmed [19]. Murray’s law generalizes to a power law

$$t^p = b_1^p + b_2^p; \quad 2 \leq p \leq 3. \quad (1)$$

Qualitatively, this law expresses that the greater the exponent value, the less the required trunk diameter, relative to branch diameters. For the greater flow rates and pipe diameters of the turbulent flow regime, p can be derived as 2.33, again with empirical confirmation [19]. Although constructed originally for diverging flow at a branching, the model also can approximate the case of converging flow. For turbulent flow in the open channels of river drainage systems (again, both fan-out and fan-in) the power law (1) is derivable, with simplifying assumptions, for $p = 2.17$ [20].

Flow phenomena have long been observed in both dendrites and axons [21], particularly during their development, although of course they have highly complex internal structure, not an unobstructed lumen. We evaluated the goodness of fit of the power law for the trunk and branch diameters of the 217 neuron arbor junctions reported by Cherniak [1]. The neuronal “tubes” are of 1–10- μm diameter range; hence the predicted exponent value for the power law would be the laminar regime $p = 3.00$. As Fig. 4 shows, the data are in fact consistent with that prediction. With mean $(b_1^3 + b_2^3) / t^3 = 1.12 (\pm 0.46)$, the neuron branch-junction data fit the laminar power law almost as well as the mouse cortex 10–100- μm -diameter arteriole branch-junction data of Wang *et al.* [22], where mean $(b_1^3 + b_2^3) / t^3 = 1.08 (\pm 0.05)$. In addition, the neuron data consistently conform to the power law better for $p = 3.00$ than for $p = 1.50$; the latter is in fact identical with the “ $\frac{3}{2}$ rule” for motor neuron dendrite trunk and branch diameters, derived from an electrotonus model [23]. The power law shows a lower error with $p = 3.00$ than with $p = 1.50$ for each of 17 of the 20 dendrite-junction groups of Cherniak [1], which is significant ($p < 0.01$) by a sign test. (The three groups that are exceptions fall into no particular pattern, but it should be noted that none of the 20 groups consisted of spinal motor neuron dendrites.) The laminar value of $p = 3.00$ also outperforms a “conservation of cross-section area” value of $p = 2.00$ [24] for 16 of the 20 groups ($p < 0.02$).

Fluid statics. Without reference to a fluid-mechanical model, a general local optimization law can be derived that relates weights of a trunk and its two branches to the

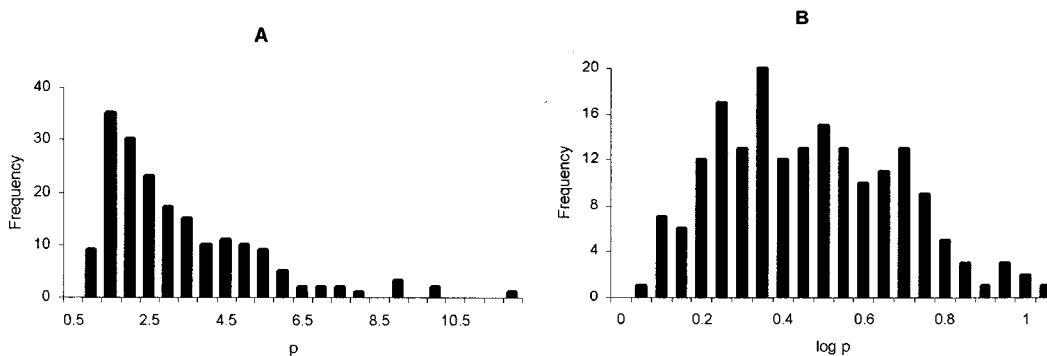


FIG. 4. Best fit of the fluid-dynamic model for dendrite and axon Y trees. The fluid-dynamic power law relating branch diameters to trunk diameter, for minimal wall drag of pumped flow at a junction, is $t^p = b_1^p + b_2^p$ (for the laminar flow regime, $p = 3.00$). The histograms are for the frequency distribution of values of the best-fit exponent p for 217 neuron junctions. (A) The raw data are skewed. (B) The \log_{10} -transformed data better approximate a normal distribution (as confirmed by linear regression analysis of a $Q-Q$ normality test); the inverse of the mean of log-transformed best-fit exponents is $3.09 (\pm 1.61)$, which approaches the laminar regime value of p . For the 173 dendrite junctions of the total data set, $p = 2.96 (\pm 1.54)$. (The neuron junction data were described in Ref. [1].)

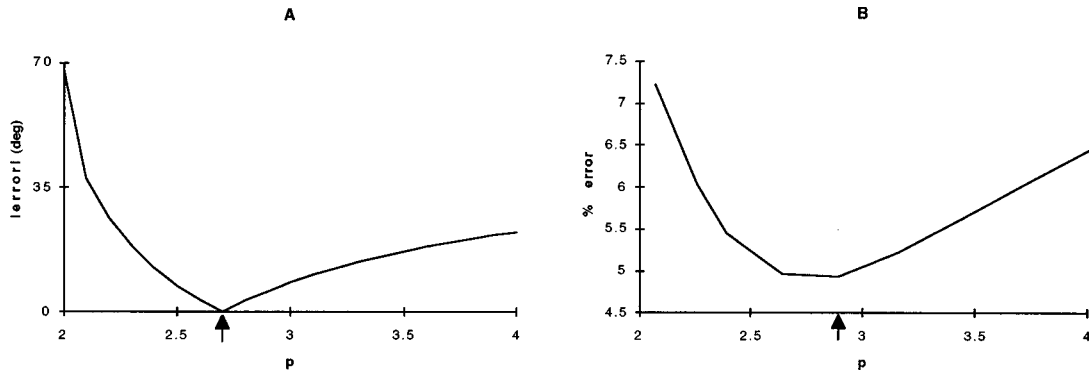


FIG. 5. (A) Combined “fluid dynamic and static model” applied to isolated dendrite Y trees (junctions from Ref. [1], p. 506). (1) The fluid dynamic power law relating branch and trunk diameters for minimization of the wall drag of pumped flow is $t^p = b_1^p + b_2^p$ (see Fig. 4). (2) The fluid-static law for the minimal tree cost is $\cos \theta = (w_t^2 - w_{b_1}^2 - w_{b_2}^2) / 2w_{b_1}w_{b_2}$, with w_n the cost per unit length of a branch or trunk; this is equivalent to the triangle of forces law of vector mechanics. The combined “ d^p & $\cos \theta$ ” model employs observed branch diameters at a junction to derive the predicted trunk diameter, then uses those three values to derive the optimal branch angle. In the above plot, there is a minimum-volume-cost point within the interpretable 2.00–3.00 range; for a cost=volume assumption, the best-fit p value of the combined model for 173 dendrite junctions is at $p=2.70$. At the best fit p , the mean error (of 0.20°) between actual observed vs predicted optimal branch angles is in fact slightly less than the mean error of the fluid-static model alone using directly observed trunk diameters (0.50°). (B) The same combined model, extended to dendrite “triads” of three interconnected Y trees (see Table I), via the STRETCH embedding-optimizer algorithm. For cost=volume, the best-fit value for five dendrite sample groups with 72 triads total is at $p=2.90$, with a mean actual topology error of 4.50% between the actual triad volume and minimal triad volume. The model for triads includes a correction for the observed bend-in of branches of each type (the model for Y trees did not). See text for branch and trunk costing procedures.

minimum-cost angle θ between the branches for connecting the trunk origin to the branch termination sites:

$$\cos \theta = \frac{w_t^2 - w_{b_1}^2 - w_{b_2}^2}{2w_{b_1}w_{b_2}}. \quad (2)$$

(See Fig. 3.) An immediate question is, what is the weight w —the cost per unit of length—to be minimized? As discussed in Ref. [1], the hypothesis that the total volume of Y junctions is minimized, rather than the surface area or length of the tree structures, is strongly confirmed for a variety of dendrites and axons. The cosine law (2) is identical to the “triangle of forces” law of vector mechanics, expressing the least-energy state of three cords fastened together at a common junction, with actual weights pulling each of them. If a Y tree is interpreted as a fluid-static system of flexible but relatively inelastic-walled tubes “inflated” at an arbitrary pressure, then the forces exerted on the cross-sectional disks of each tube will in fact drive the junction to an energy-minimization angle that is identical with the angle for minimization of volume (but not of surface area or of length). Thus, via a tug of war process, fluid statics provides a mechanism for the local optimization of arbor volume.

Since tree volume is a function of branch and trunk diameters, the fluid-dynamic power law and the fluid-static cosine law can be linked in a single fluid-mechanical model. In effect, a “ d^p & $\cos \theta$ ” local model accepts the two branch diameters at a junction and outputs the trunk diameter and the volume-minimizing branch angle. The combined model also implies, qualitatively, that the smaller the p value, the smaller the branch angle θ . Figure 5(A) shows that the combined model performs at least as well at predicting dendrite junction angles as the cosine law alone (reported in Ref. [1]), with quite low mean errors. A discrepancy may be perceived between the best fit $p=2.96$ of the power law to the dendrites (Fig. 4), versus the best-fit value $p=2.70$ of the com-

binated model in Fig. 5(A); the combined model p value falls virtually in the middle between the 3.00 laminar regime value and the 2.33 turbulent value. One explanation of the lower p value of the combined model is branch bend-in: As discussed below, almost all types of naturally generated tree structures show some inward curvature of branches as they leave the immediate junction zone. Branch angles of the Cherniak [1] data were measured at approximately one trunk diameter from the junction zone, and so reflect some amount of branch bend-in; observed angles will therefore be somewhat lower than the most immediately local ones. As indicated above, the best fit p will correspondingly be decreased. An estimate of the extent of branch bend-in for the Cherniak [1] data, derived from the “true” local 2.96 p value directly based on the power law alone, and the 2.70 p value of the combined model, is 7.1° , which is consistent with the much greater bend-in observed for branches at ranges further from the junction.

MULTIJUNCTION TREES

The Y trees of the above analysis can be viewed as components of more complex trees, such as “triads” consisting of three interconnected Y trees. However, local optimization does not entail global optimization. In particular, the terminal set of a Y tree has only one possible topology, while larger terminal sets have an exponentially growing number of alternative topologies (see Ref [7], Table 1.1). The cosine law above expresses only the minimum-cost local embedding or “stretching” of the Y-tree topology. First, the embedding concept must be generalized to the global topologies of more complex trees, with branches of varying weight, or cost per unit length.

Embedding a topology. Optimization of large-scale embedding can again be conceived of in terms of the idea of a tree as a system of laminar-regime tubes in a vector-

mechanical tug of war. Vector-mechanical treatment of tree networks of weight-loaded cords with as many as five internodal junctions appeared in work by Varignon [25]. Huang and Kahng [26] developed for us an algorithm to derive the minimum-total-cost embedding of a variably weighted Steiner tree, with affinities to a concept by Gilbert [27]. We employed this algorithm in a tree embedder, STRETCH: A tree such as in Fig. 2(B) is represented as an input file, specifying its topology (i.e., the connections among node and junction sites), with coordinates of the root and leaves, and of the observed internodal junctions, and weights of each branch. STRETCH proceeds from junction-linked leaf pairs inward. Using the cosine law above, STRETCH finds the minimum-cost site of the internodal junction for each leaf pair. It then in turn treats these internodal junctions as second-order leaves, and finds the minimum-cost junction sites for these new “leaves.” The algorithm continues back in this way, also testing junction mergings, until it reaches the root. The output is the optimal embedding of the tree, represented as loci of the internodal junctions; Fig. 2(C) depicts a typical minimum-cost embedding, for volume. STRETCH can be set to minimize the total volume, surface area, or branch length of a tree.

Neuron arbor data were scanned from published Golgi and HRP camera lucida drawings. The span of complete arbors ranges well above 100 μm ; since branch diameters are below 10 μm , these images rarely include accurate representations of branch diameter [see, e.g., Fig. 2(A)]. Given the good confirmation described above of the laminar power law for the neuron Y trees, we instead employed it to estimate diameter costs of triad branches. Like STRETCH, the “coster” algorithm proceeds from the leaves inward: Branch tips are assigned a uniform cost of 1; at their junctions, the power law is used to assign cost to the trunks. Thus, for p set at 3.00, the assigned trunk cost is not 2, but 1.26. The costing procedure progresses iteratively back to the root node.

Observed branch bend-in was also incorporated into the model: For naturally occurring trees, if branch angles are measured at the maximum distance from the junction site—that is, with each branch defined by the segment from the junction out to its termination (either at a leaf site or a next outermost junction)—the angles are consistently less than angles measured as close as feasible to the junction point. While branches vary in sinuosity, such bend-in appears virtually as ubiquitous among dendrites and axons, living and nonliving natural trees, as conformance to the power law or the cosine law: We have observed it for arteries and veins, plant arbors, river drainage networks (both fan-in and fan-out), and electric discharge tree patterns. The mean branch bend-in for the 72 dendrite triads analyzed here is 24.3° (± 19.3); for the 32 axon triads, it is 12.9° (± 24.4). (One possible general explanation for all of these cases is in terms of a constant modulus of elasticity for branch walls.) Since the power and cosine laws only apply locally, in the immediate junction neighborhood, the observed mean bend-in for each class of dendrites and axons was used to correct—i.e., decrease—the laminar p value of 3.00 for predicting the angle of the full length of the branches. [The labels in Fig. 2(B) show the assigned branch costs to a triad, with correction of $p=3.00$ by the mean branch bend-in of 25.9° for the class of rabbit α ganglion dendrites.]

At $p=3.00$, the observed embeddings of the 104 actual neuron triads have a mean volume cost that is 5.40% (± 3.80) greater than the minimum cost of the optimal embeddings of their actual topologies. [The axon error of 5.78% (± 4.56) runs somewhat greater than the dendrite error of 5.05% (± 3.07).] For p instead set at the turbulent-flow-regime value of 2.33, the mean neuron error rises to 6.31% (± 4.96). This difference is small but consistent: The error at 3.00 runs below the error at 2.33 for seven of the eight neuron groups; of the 104 individual triads, 68 show less error at 3.00 than at 2.33, a highly significant effect ($p < 0.001$, $r_m > 0.31$). For comparison, the corresponding mean embedding error is similar, 4.42%, for eight triads from artificially generated streams [28] and eight triads from the Mississippi River delta [29], with p at the 2.17 value derived for turbulent flow in open channels, as explained earlier. With p at the 2.33 turbulent value, 24 human coronary artery triads [30] (having a 2.45-mm mean trunk diameter) show a mean embedding error of 4.49%; 20 of 24 better fit the turbulent than laminar p value, which is again significant ($p < 0.01$). As noted by Cherniak [1] for local junction geometry, these comparable errors are consistent with the hypothesis that the global neuron arbors, like the fluid networks, are created by simple fluid-mechanical processes.

Table I shows the mean best-fit value of p for each arbor class, that is, the p value (with correction for mean branch bend-in) at which the embedding volume error of the topologies of the set of actual arbors (“VL error”) is minimized. The first observation is that every triad group, living and nonliving, has a best-fit value p , $2 < p < 4$; that is, there exists a minimum-volume cost point above 2.00 and below 4.00 (for the dendrite group, see Fig. 5). The mean embedding error for neurons drops some to 4.80%, with the mean best-fit value p at 2.92—agreeing well with the fluid-mechanical hypothesis that the neuron arbors behave like laminar-flow-regime pipe networks. Furthermore, the laminar behavior is consistent: as can be seen, the mean best-fit value p is closer to 3.00 than 2.33 for seven of the eight neuron groups. Finally, the volume-cost hypothesis outperforms both the surface area and the length hypotheses for all eight neuron groups. Similarly, for 95 of the 104 triads, their individual best-fit minimum-error values for volume costing are lower than the best-fit error values for surface area or for length.

To provide measures of variance, corresponding means for the pooled individual triad data are: for the 72 dendrites, a best-fit value p of 3.38 (± 1.39), with a volume error of 3.58% (± 2.82); for the 32 axons, a best-fit value of p of 3.20 (± 1.17), with a volume error of 3.97% (± 3.33); and for all 104 neuron arbors, a best-fit value of p of 3.33 (± 1.33), with a volume error of 3.70% (± 2.99). While the variance here is appreciable, conformance to the laminar over the turbulent model is consistent; independent lines of evidence converge in supporting the laminar model—in particular, both local and direct measurements of branch diameters at junctions (Fig. 4), as well as the global arbor analysis here.

Searching topologies. Finding the minimum-cost large-scale embedding of a given tree connecting a node set does not suffice for finding the optimal tree for the node set. The best embedding of the given tree topology may in effect constitute only a local minimum trap on the optimization

TABLE I. Global optimization of neuronal and non-neuronal arbors. Each arbor sample is a “triad,” a tree with three internodal junctions; see Fig. 2. The mean percent error of a triad group is in terms of the cost of each actual tree compared with its corresponding optimized tree [expressed as “(Actual-Optimal)/Optimal”]. All actual vs optimal tree errors are for the best-fit value of exponent p in the fluid-dynamic power-law model relating branch and trunk diameters at junctions: that is, the p value at which the mean embedding errors of the actual trees, for the volume cost, are lowest. That best-fit value of p , with a correction for the observed branch bend-in angle, is given for each triad group. Next listed is the mean percent error of each triad’s actual topology in its actual embedding, vs the actual topology in its cheapest volume-cost embedding. In addition, the performance of actual trees relative to the corresponding minimum-cost topology is evaluated for the hypotheses that minimized cost is equal to total volume (VL), surface area (SA), and length of arbor (LG). To find optimal tree topologies, all 15 possible triad topologies (see Fig. 6) were searched: The mean volume cost-rank of the actual tree’s topology when the optimally embedded (Topol rank), in comparison with the volume costs of every other topology optimally embedded is given. All samples conform best to a volume-minimization model. River network triads also minimize volume comparably, which is consistent with the idea that both neurons and water networks achieve such optimization by fluid-mechanical processes. In addition, optimization of the topology gains little, compared with optimization of the embedding.

Triad set	Actual topology			Optimal topology		
	Best-fit p^a	VL error	Topol rank	VL error	SA error	LG error
Neutron arbors						
Dendrites						
Alpha ganglion, rabbit ($n=23$) [13]	2.58	4.22	3.39	4.92	22.68	52.57
SD		± 2.96	± 2.54	± 3.30	± 12.52	± 26.61
Alpha ganglion, cat ($n=12$) [32]	2.83	6.09	3.58	7.64	17.64	36.15
SD		± 3.94	± 2.71	± 3.84	± 6.62	± 17.00
Delta ganglion, cat ($n=8$) [32]	2.94	5.86	2.88	7.36	16.31	33.30
SD		± 3.72	± 2.42	± 4.00	± 7.05	± 14.54
Parasol, human ($n=21$) [33]	3.33	4.45	1.43	4.59	7.25	12.42
SD		± 2.86	± 0.81	± 3.03	± 5.51	± 8.10
Starburst amacrine, rabbit ($n=8$) [34]	2.72	1.68	3.63	1.86	24.13	63.70
SD		± 1.03	± 1.92	± 0.93	± 11.77	± 28.02
Dendrite group means ($n=72$)	2.90	4.50	2.82	5.21	16.79	37.22
Axons						
Intrinsic, thalamus, mouse ($n=8$)	3.65	5.18	1.63	5.88	8.27	12.58
SD		± 3.02	± 1.77	± 4.48	± 5.87	± 11.12
Extrinsic, thalamus, mouse						
Cortical ($n=19$)	2.72	5.11	2.11	5.40	11.63	19.87
SD		± 4.48	± 1.79	± 4.45	± 7.41	± 11.87
Ascending RF ($n=5$) [35]	2.88	7.29	1.60	7.92	15.84	31.17
SD		± 5.58	± 0.55	± 5.40	± 8.04	± 17.52
Axon group means ($n=32$)	2.98	5.47	1.91	5.92	11.45	19.81
Neuron group means ($n=104$)	2.92	4.80	2.54	5.43	15.15	31.86
Non-neutron arbors						
Human coronary arteries ($n=24$) [30]	2.44	4.55	2.00	4.85	21.45	52.93
SD		± 3.54	± 1.41	± 3.51	± 9.83	± 22.15
River drainage network, artificial ($n=8$) [28]	2.54	3.87	1.38	3.94	12.19	28.85
SD		± 2.58	± 0.52	± 2.58	± 6.57	± 12.34
River delta, Mississippi ($n=8$) [29]	2.12	3.41	4.25	3.55	27.15	69.86
SD		± 3.77	± 1.83	± 3.82	± 11.37	± 25.42
Weight-table network ($n=24$)	3.00	0.06	1.25	0.21	3.53	17.34
SD		± 0.04	± 0.85	± 0.21	± 1.29	± 7.03

^aSince each triad group p is the best-fit value for that arbor group, these p values have no SD. Dendrite, axon, and neuron p value means are weighted averages of the best-fit p values of their respective groups (see text for means of pooled individual data).

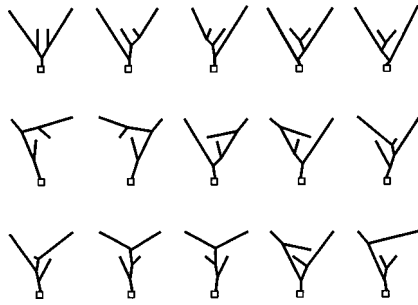


FIG. 6. The 15 alternative possible topologies, or connecting patterns, for a “triad,” a five-terminal tree with three internodal junctions. Steiner tree optimization of an arbor requires not just (a) the best embedding of the arbor’s actual topology [i.e., the lowest-cost positioning of its internodal junctions, as in Fig. 2(C) vs 2(B)], but (b) an exhaustive search of all possible topologies connecting the terminals to find the one that is cheapest when best embedded [as in Fig. 2(D) vs 2(C)].

landscape [compare, for example, Figs. 2(C) and 2(D)]. Under the standard conception, a topology is the structure that remains invariant under continuous stretching transformations (i.e., without tearing or joining); two topologies are distinct if one cannot be converted into the other by any embedding operation. Therefore, to find the global minimum, every possible alternative topology interconnecting the node set must be generated and then embedded. Figure 6 shows the 15 possible topologies for the node set of a triad. (The triad data of Table I were sampled across all the main types of topologies.)

We constructed a “TG→Coster→STRETCH” package: First, TG is given a tree input file like that described for STRETCH, and generates each possible alternative full topology for the given node set. Once TG has created a particular such connecting pattern, the Coster program described above assigns branch weights according to a specified exponent setting of the power law. The resulting tree file is then sent to STRETCH to find its optimal embedding. Statistics are accumulated on both optimal and “pessimal” optimally embedded topologies, that is, the cheapest and costliest topologies after their embeddings have been minimized.

Performance of the optimal topologies closely parallels that of the actual topologies. Again, for every neuron group, the volume-cost error is always considerably less than surface area-cost error, which in turn is always less than length-cost error; the neurons still appear to be minimizing volume. As can be seen in Table I, the mean volume error (at the best-fit value p) for actual neuron topologies of 4.80% only increases to 5.43% for the optimal topology. [Correspondingly, means for pooled individual neuron triad data show the same pattern, increasing from 3.70% (± 2.99) to 4.53% (± 3.62).] That is, perfecting the embedding of the actual topology gains considerably more in volume cost than perfecting the topology itself. While there are only 15 alternative tree topologies for a five-node set, the same “unimportance” of topology selection relative to embedding also applies for larger node sets with much greater numbers of alternative topologies—e.g., for eight-node sets, which have 10 395 alternative topologies; and nine-node sets, which have 135 135 topologies (see, e.g., Figs. 7 and 8). In addition, performance of the actual neuron topology, optimally

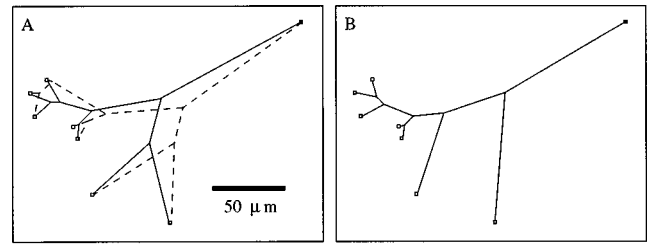


FIG. 7. Eight-terminal arbor of extrinsic axon (ascending reticular formation), mouse thalamus (from Ref. [35]). (A) Wireframe representation of the observed arbor. The actual topology, with the observed embedding of that topology, appears in broken lines. The optimal embedding with respect to volume minimization of the actual topology is superimposed in solid lines. [Branch costing is via the power law, with p set at the best-fit value (with a branch bend-in correction) for this arbor group in Table I.] The cost in volume of the actual arbor exceeds that of the optimal embedding of its topology by 2.20%. (B) “Best of all possible topologies” connecting the given terminal loci: the optimal topology with respect to volume, optimally embedded. The cost in volume of the actual arbor exceeds that of the optimal topology by 2.47%. Only ten of the 10 395 possible alternative topologies have lower total volume costs, when optimally embedded, than the actual topology.

embedded, relative to all other topologies appears to be invariant across the three cost measures: the mean relative rank of the actual triad topology varies only slightly for the different cost measures (2.84 for volume, 2.55 for surface area, and 2.62 for length). Finally, their similar actual topology ranks in Table I suggest that neuron arbors are not “smarter” than the nonliving river networks at finding the cheapest-volume topology, this despite the well-known remodeling processes acting upon many types of dendrites and axons, such as synapse and branch pruning.

Benchmarks. Thus neuron triads minimize their volume to

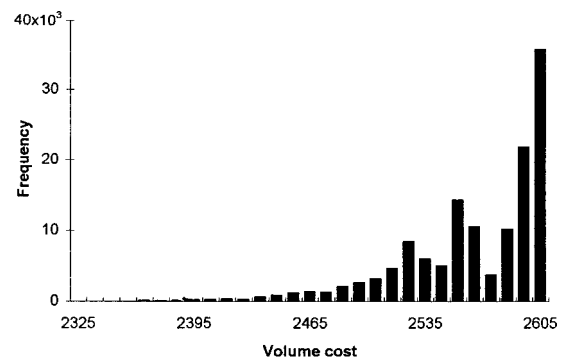


FIG. 8. Distribution of volume costs of all possible topologies, each optimally embedded, of a nine-terminal extrinsic axon arbor, mouse thalamus (from Ref. [35]). The histogram shows the usual pattern for natural arbors, living and nonliving: the more costly topologies are more common, the cheapest ones are the rarest. Consequently, the good topology selection of the natural arbors cannot result merely from a confound that the least costly layouts occur most frequently. The histogram was compiled from an exhaustive search of all 135 135 alternative topologies for a nine-terminal Steiner tree, requiring about five days on a P6 400-MHz computer. The most costly optimally embedded “pessimal” layouts have only about 12% greater volume than the cheapest one; in this sense, for optimization, “topology does not matter.”

within about 5% of the corresponding optimal trees. For sociological comparison, rectilinear Steiner trees for very large-scale integrated microcircuit chip layout are regarded in the industry today as well minimized if they come within 10% of optimum length (see, e.g., Ref. [7], pp. 221–242). We have also noted that river networks typically are a couple of percent closer to optimum than the neurons; since the river branch data ranges above 1-km scale, while the neuron data are at the 1- μm scale, simple measurement error may be responsible for the somewhat greater neuron optimization error. Table I includes a benchmark: data for a set of weights and pulleys tree networks constructed with interconnected force tables. In effect, these triads are “pure” vector-mechanical trees, as in Varignon [25]—a type of analog computing device for the embedding problem. Their branch loadings were set for “volume” minimization, with $p = 3.00$ for the power law relating branch and trunk costs; the loci of the internodal junctions were than “read out.” A variety of topologies and leaf loadings were sampled. The optimal-topology volume error drops by an order of magnitude, to 0.21%; however, the topology rank improves only moderately over some neuron and river groups.

The force-table triads also serve as a calibration of the optimization assessment procedures here. The best-fit p value for their internodal junction loci does indeed turn out to be at 3.00; also, surface area and length errors come out much greater than the volume-cost error. In addition, four triads of conventional minimum-length Steiner trees (from Refs. [9,11]) were scanned in and evaluated with the TG-STRETCH package. For the optimal topology, the mean length error for the actual triads was 0.22%, about the same as the force-table error. In addition, these “near-perfect” minimum-length trees each showed markedly worse volume and surface area errors (for example, at $p = 3.00$, the respective mean errors were 7.42% and 1.56%). Thus the procedures here did in fact detect that these test samples were minimizing length, not volume or surface area. Another calibration strategy is to generate the “perfect” minimum surface area tree for the nodes of some actual triad, then in turn test the assessment procedures on this optimum actual tree as an input. For one such minimum surface area dendrite tree (at $p = 3.00$, with 16° bend-in), the optimal-topology surface area error was indeed only 0.000 005%, while the volume error was 1.61%, and the length error was 0.92%.

In judging how good is “good,” benchmarks from the other extreme are useful comparisons. Mean optimal volume embedding of the “pessimal” topology for neuron triads—the topology that is costliest when minimum-cost embedded—costs only 1.81% more than the corresponding actual topologies in their actual embeddings, while the optimal embedding of the optimal topology costs 5.43% less. So, again, topology makes little difference. For larger node sets, for example, nine-node trees, a histogram shows the distribution of costs of all 135 135 topologies, optimally embedded (see Fig. 8): The cheapest vs costliest topologies differ by only $\sim 13\%$, a strikingly narrow range over so many alternative topologies. A next question concerns how much is at stake instead with embedding. Bad embeddings of four neuron triad node sets were constructed “by hand,” under the constraints of no branch crossovers and no internodal junctions outside the convex hull of the terminals, with a

junction costing at $p = 3.00$ (corrected for the observed branch bend-in); each cost about twice as much in volume as the corresponding actual neuron triad. Even such an informal approach indicates how much embedding, unlike topology, can matter.

Finally, is the optimization behavior of larger-sized neuron trees similar to that of triads, i.e., five-node trees?. The size limit of currently feasible topology searches is nine nodes; a ten-node tree has 2 027 025 alternative topologies. As for triads, volume minimization dominates for larger trees (mean optimal topology errors for nine-node neuron trees are 10.28% volume, 14.86% surface area, and 23.07% length). As for triads, an optimal topology gains relatively little improvement over the actual topology (for the nine-node trees, the actual topology volume error is 8.19%, only slightly less than the optimal-topology error). Larger trees do show a pair of salient differences from triads: The embedding volume-minimization error tends consistently to increase with node-set size, from 4.80% for triads to $\sim 8\%$ for the nine-node arbors. Conversely, the topology rank error of the actual tree drops sharply, from the top 10.93% for triads to 1.02% for the nine-node arbors.

The basic point here has been that major neuron arbor structure appears to be self-organizing, with both dendrite and axon morphogenesis behaving like flowing water. Neuron arbor anatomy fits a global volume-minimization model nearly as well as nonliving tree structures such as river drainage networks. Ramón y Cajal observed that a developing axon tends to grow in a straight line, as long as it does not encounter interfering environmental influences [21,31]. The account of neuron arbor morphogenesis here can be viewed as a generalization of this idea: The default axodendritic arbor pattern, when external cues do not intervene, is the volume-minimizing embedding. This optimal-volume structure is conceived to be a basic ground plan, an *ur* arbor often modified in complex ways—for example, as manifested in the tortuosities typical of intrinsic cortical axons.

The simple “neural fluid mechanics” described above generates this default arbor structure, in particular, branch diameters, branch angles, and junction sites. Since river networks perform as well at topology optimization as dendrites and axons here, DNA-based mechanisms do not seem to be required. The significant role of basic properties of micron-scale fluid flow behavior in neuron arbor formation draws attention to the idea that modulators of the fluid-mechanical milieu of the nervous system may govern aspects of its normal development. Modification of such properties as viscosity or surface tension therefore may be worth investigation—for example, toward promoting connection regrowth after injury.

ACKNOWLEDGMENTS

We thank Jen-Hsin Huang and Andrew Kahng for indispensable assistance in the conceptual development of the STRETCH embedding algorithm. Athanassios Dimas derived the fluid-dynamic models for turbulent flow in open channels. Dennis Dacey, Edward Famiglietti, Robert Marks, Robert Rodieck, and Arnold Scheibel gave valuable neuroanatomical advice. In addition, we are grateful for the help of Carl Rovainen and Stanley Schumm, and Kelly Changizi, Michael Gurevich, Nancy Hall, and Sara Volmer. The work was supported by NIMH Grant No. MH49867.

- [1] C. Cherniak, University of Maryland Institute for Advanced Computer Studies Technical Report No. 90-90, 1991; *Biol. Cybern.* **66**, 503 (1992).
- [2] C. Cherniak, University of Maryland Institute for Advanced Computer Studies Technical Report No. 91-98, 1991; *J. Neurosci.* **14**, 2418 (1994); *Trends Neurosci.* **18**, 522 (1995).
- [3] D. Thompson, *On Growth and Form* (Cambridge University Press, New York, 1917).
- [4] S. Kauffman, *At Home in the Universe* (Oxford University Press, New York, 1995).
- [5] C. Cherniak, M. Changizi, and D. Kang, University of Maryland Institute for Advanced Computer Studies Technical Report No. 96-78, 1996.
- [6] C. Mead, *Analog VLSI and Neural Systems* (Addison-Wesley, Reading, MA, 1989).
- [7] F. Hwang, D. Richards, and P. Winter, *The Steiner Tree Problem* (North-Holland, Amsterdam, 1992).
- [8] D. Du and F. Hwang, *Algorithmica* **7**, 121 (1992).
- [9] H. Lewis and C. Papadimitriou, *Sci. Am.* **238**, 96 (1978).
- [10] M. Garey and D. Johnson, *Computers and Intractability: A Guide to the Theory of NP-completeness* (Freeman, San Francisco, 1979).
- [11] M. Bern and R. Graham, *Sci. Am.* **260**, 84 (1989).
- [12] G. Mitchison, *Proc. R. Soc. London, Ser. B* **245**, 151 (1991).
- [13] L. Peichl, E. Buhl, and B. Boycott, *J. Comp. Neurol.* **263**, 25 (1987).
- [14] D. Hillman, in *Intrinsic Determinants of Neuronal Form and Function*, edited by R. Lasek and M. Black (Liss, New York, 1988), pp. 83–113.
- [15] D. Purves and J. Lichtman, *Principles of Neural Development* (Sinauer, Sunderland, MA, 1985).
- [16] L. Peichl, H. Ott, and B. Boycott, *Proc. R. Soc. London, Ser. B* **231**, 169 (1987).
- [17] C. Murray, *Proc. Natl. Acad. Sci. USA* **12**, 207 (1926).
- [18] V. Streeter and E. Wylie, *Fluid Mechanics*, 8th ed. (McGraw-Hill, New York, 1985).
- [19] M. LaBarbera, *Science* **249**, 992 (1990).
- [20] A. Dimas (unpublished).
- [21] R. Lasek, in *Intrinsic Determinants of Neuronal Form and Function* (Ref. [14]), pp. 3–58.
- [22] B. Wang, N. Blocher, M. Spence, C. Rovainen, and T. Woolsey, *J. Cerebral Blood Flow & Metabolism* **12**, 935 (1992).
- [23] W. Rall, *Exp. Neurol.* **1**, 491 (1959).
- [24] D. Hillman, in *The Neurosciences*, edited by F. Schmitt and F. Worden (MIT Press, Cambridge, MA, 1979), Chap. 27.
- [25] M. Varignon, *Nouvelle Mecanique* (Claude Jombert, Paris, 1725), Vols. 1 and 2.
- [26] J.-H. Huang and A. Kahng (unpublished).
- [27] E. Gilbert, *Bell Syst. Tech. J.* **46**, 2209 (1967).
- [28] S. Schumm, M. Mosley, and W. Weaver, *Experimental Fluvial Geomorphology* (Wiley, New York, 1987).
- [29] T. Elliott, in *Sedimentary Environments and Facies*, 2nd ed., edited by H. Reading (Blackwell, Oxford, 1986), Chap. 6.
- [30] M. Changizi and C. Cherniak, *Modeling Large-Scale Geometry of Human Coronary Arteries with Principles of Global Volume and Power Minimization* (Committee on History & Philosophy of Science, University of Maryland, College Park, 1998).
- [31] S. Ramón y Cajal, *Degeneration and Regeneration of the Nervous System*, translated by R. May (Oxford University Press, London, 1928).
- [32] D. Dacey, *J. Comp. Neurol.* **288**, 59 (1989).
- [33] D. Dacey, *Visual Neurosci.* **10**, 1081 (1993).
- [34] E. Famiglietti, *Brain Res.* **261**, 138 (1983).
- [35] M. Scheibel and A. Scheibel, *Brain Res.* **1**, 43 (1966); *The Neurosciences*, edited by F. O. Schmitt (Rockefeller University Press, New York, 1970), Chap. 41; A. Scheibel, in *Handbook of Physiology—The Nervous System*, edited by I. Darian-Smith (American Physiological Society, Bethesda, MD, 1984), Vol. 3, Pt. 1, Chap. 6.